THE ASTROPHYSICAL JOURNAL, 403:396–411, 1993 January 20

THE DISTANT FUTURE OF SOLAR ACTIVITY: A CASE STUDY OF β HYDRI. II. CHROMOSPHERIC ACTIVITY AND VARIABILITY[1]

D. DRAVINS,[2] P. LINDE,[2] K. FREDGA,[3] AND G. F. GAHM[4]

Received 1992 January 28; accepted 1992 July 23

ABSTRACT

The secular evolution of solar-type chromospheres is studied through a detailed comparison of the present Sun (G2 V) with the very old ($\simeq$9.5 Gyr) star β Hyi (G2 IV). In such old stars one might observe the lowest possible levels of stellar activity. Detailed studies of various atmospheric layers in β Hyi have been made, and this Paper II in the series treats chromospheric features and their time variability. High-resolution Ca II H and K profiles show the emission about half that for the Sun, but with the same sense of violet-red asymmetry (the shortward peak the strongest). The emission's wavelength width is slightly broader, consistent with the Wilson-Bappu relation for this slightly more luminous star. Mg II *h* and *k* profiles also show an emission weaker than in the Sun, but with the opposite sense of asymmetry, probably altered by absorption in a nearby interstellar cloud. The Mg II variability was monitored from the *IUE* satellite during about 12 yr, recording some 100 high-resolution line profiles. Accurate spectrophotometry is assured by recently developed *IUE* image processing techniques. The emission variations are small ($\lesssim$30% in Mg II *h* and *k*) and are characterized by smooth and systematic changes in the line profiles from year to year, suggesting continuous changes in the chromospheric structure, rather than the sudden emergence or growth of active regions. These 12 yr embrace both an activity minimum and a maximum, consistent with an activity cycle somewhat longer ($\simeq$15–18 yr) than the solar one. Assuming the Ca II emission variation to follow that of Mg II, the corresponding peak-to-peak amplitude in the Mount Wilson K-line index would be on the order of 1%, making this the lowest amplitude stellar activity cycle so far detected.

Subject headings: stars: chromospheres — stars: individual (β Hydri) — Sun: activity —ultraviolet: stars

1. THE EVOLUTION OF SOLAR-TYPE CHROMOSPHERES

In this series of papers, the very old solar-type star β Hyi (HR 98 = HD 2151; G2 IV) is examined in detail as a likely proxy for the future Sun, in order to find a probable scenario for the state of solar activity in the distant future, when the Sun has reached twice its present age and started its evolution off the main sequence. The basic properties of β Hyi were examined in Paper I (Dravins et al. 1993a), where it was found to be a fully normal single star, of age 9–10 Gyr, evolved from nearly the same position as the Sun's zero-age main-sequence location. Any small difference is consistent with the small metallicity difference—β Hyi is slightly metal poor, as is normal for stars of the old disk population.

It is well known that Ca II H and K emission on the Sun coincides with photospheric magnetic fields, and that brighter emission accompanies larger field strengths. Individual solar features show emission patterns in Ca II, Mg II, Lyα, and other lines, whose shapes and strengths generally show a close correlation (e.g., Bonnet 1981). Their time variability in integrated sunlight reflects the modulation due to solar rotation, the changing number of active regions, and more general changes during the activity cycle.

This paper (Paper II of the series) concerns itself with such activity indicators, and their time variability. It is organized as follows. Section 2 describes various chromospheric signatures in β Hyi, comparing them to those in the spectrum of integrated sunlight, and explaining our various methods of observation. Section 3 analyzes the time variability in Mg II *h* and *k* emission fluxes and line profiles while § 4 concludes with an outlook for future studies. The Appendix gives an account of the data analysis procedures developed for precision photometry of spectra from the *IUE* satellite. The transition region and corona will be treated in Paper III of this series (Dravins et al. 1993b).

2. CHROMOSPHERIC INDICATORS

Old stars tend to have less chromospheric activity than young ones, and β Hyi is no exception. A not uncommon belief is that the outer atmospheric emission from cool stars comprises two parts: one "basal" component, independent of stellar magnetic activity, and another "magnetic" component (e.g., Schrijver 1987). The basal flux component could result purely from acoustic heating, while the flux in excess of it would have its origin in magnetohydrodynamic processes. The "excess" line fluxes from different temperature regimes have been shown to be highly correlated for dwarfs and giants alike, suggesting that the general structure of the outer atmosphere is similar for a wide variety of stars. If correct, this means that considerable insight into the structures of stellar outer atmospheres can come from a detailed study of a few (representative) stars only. Studies of chromospheric activity versus stellar age further suggest that the age-activity relation for solar-type stars is *deterministic*, and not merely statistical (Soderblom, Duncan, & Johnson 1991), again pointing at the importance of detailed case studies of well-understood stars.

Although the chromospheric emission features in β Hyi are weaker than those in the solar spectrum, they can be studied in

[1] Based on observations collected at European Southern Observatory, La Silla, Chile, and by the *International Ultraviolet Explorer*, collected mainly at the Villafranca Satellite Tracking Station of the European Space Agency.

[2] Lund Observatory, Box 43, S-22100 Lund, Sweden.
[3] Swedish National Space Board, Box 4006, S-17104 Solna, Sweden.
[4] Stockholm Observatory, S-13336 Saltsjöbaden, Sweden.

high-resolution data. In this section, we discuss various such signatures, and use them to discuss chromospheric properties in β Hyi. The collisionally dominated resonance lines of Ca II H and K, and Mg II *h* and *k* are the classical diagnostics, but also other lines contribute to the understanding of chromospheric structure.

2.1. Ca II H *and* K

This is the classical chromospheric signature. Ca II is an abundant ion in the chromosphere, and its resonance lines are very strong and readily observable from the ground. The H and K lines are collisionally excited and thermalized in the low chromosphere, and therefore emission cores will result in those atmospheric structures where there is a suitable chromospheric temperature rise with height.

2.1.1. *Observations of* Ca II H *and* K

The Ca II H and K lines in β Hyi, as well as those in integrated sunlight, were observed with the ESO 1.5 m coudé auxiliary telescope, feeding the coudé echelle spectrometer (Fig. 1). The nominal spectral resolution $\lambda/\Delta\lambda$ was 100,000 and the spectra are slightly oversampled by a Reticon 1870 element detector. The K line in β Hyi was measured on 1982 March 6 (93 minute integration), and H on March 9 (80 minutes). Identical instrumentation was used to measure integrated sunlight on March 5 (K; 10 minutes) and March 8 (H; 33 minutes). The source for integrated sunlight was the sunlight-illuminated white dome of the nearby 3.6 m telescope. (This stands higher on the mountain than the coudé auxiliary telescope, and thus can be observed by the latter.) The lower noise in the solar spectra is due to their deeper exposures.

2.1.2. *The Sun Seen as a Star*

The detailed comparison between β Hyi and the Sun is made somewhat complicated by the absence of any spectral continuum in the vicinity of the H and K lines. Although the photospheric spectra are very similar, the slightly different metallicities may somewhat change the level of the "pseudocontinuum" in the violet. Its precise placement is quite difficult even when extended spectral scans are available, as evidenced by the significantly different continuum scales in the integrated sunlight atlases by Beckers, Bridges, & Gilliam (1976) and Kurucz et al. (1984), respectively. In the absence of extended spectral scans, the solar data in Figure 1 were put on a continuum intensity scale reasonably similar to that in these atlases, and the β Hyi profiles were then normalized to the solar profiles in the outer (photospheric) wings of the H and K lines, respectively.

A comparison between the Sun and β Hyi shows that the weaker H absorption line is of comparable strength, but the stronger K line is somewhat deeper in β Hyi. The central portion of the K-line absorption flanks (i.e., outside the chromospheric features) is formed in the upper photosphere and lower chromosphere, and its flux is a measure of the temperature there. The increased depth in β Hyi might be an indication of a cooler temperature minimum in the upper photosphere and of less chromospheric heating in β Hyi. This is consistent with the suggestion by Linsky et al. (1979b), that this [K_1] minimum generally decreases with evolution away from the zero-age main sequence, thus being a measure of stellar age.

The double-peaked chromospheric emission in both H and

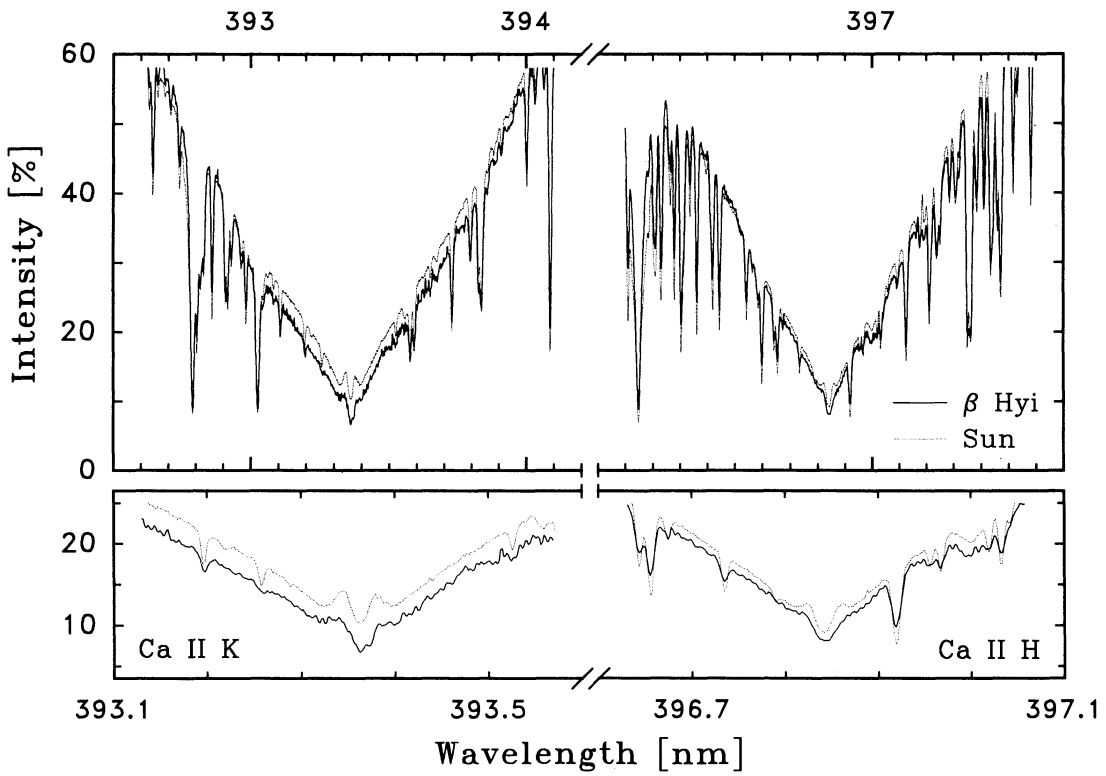

FIG. 1.—Ca II H and K lines in β Hyi (*solid*), compared to those in integrated sunlight (*dotted*), measured with identical resolution. For both H and K, the double-peaked chromospheric emission is clearly weaker in β Hyi than in the Sun, but all lines show the same sense of violet-red asymmetry. The emission's wavelength width is slightly broader, consistent with the Wilson-Bappu relation for the slightly more luminous β Hyi. The bottom panels show an expanded view of the line cores.

K is clearly weaker in β Hyi than in the Sun, but in both cases with the same sense of violet-red asymmetry (the shortward peak the strongest). For other high-resolution profiles of integrated sunlight, see White & Livingston (1981) and Oranje (1983a).

The time-averaged differences between β Hyi and the Sun are probably somewhat smaller than those in Figure 1. Anticipating a later result from our variability study, we note that the observing epoch for β Hyi happened to correspond to a Mg II emission somewhat below average, while the observing days for the Sun were characterized by a moderately high solar activity.

2.1.3. *The Wilson-Bappu Effect*

As seen in Figure 1, the wavelength width of the β Hyi emission is slightly broader than that of sunlight, consistent with the Wilson-Bappu relation for a somewhat more luminous star. Due to the weakness of emission, the precise value of the width depends rather sensitively on how the emission is defined. This increased width in β Hyi was first noted by Zarro & Rodgers (1983).

2.1.4. *Previous Observations*

The earliest Ca II K observation of β Hyi we are aware of is in the survey of southern G, K, and M stars by Warner (1969). From a photographic spectrogram, he concluded the dubious presence of an emission: strength "$\frac{1}{2}$?" on a scale between 0 and 8. A K profile at moderate resolution was published by Zarro & Rodgers (1983), while higher resolution data are in Beckman, Crivellari, & Foing (1984) and Rebolo et al. (1989). Pasquini, Pallavicini, & Pakull (1988) derived the chromospheric radiative losses, finding quite similar fluxes for β Hyi and sunlight. A comparison with our observations confirms that β Hyi did not undergo any perceptible changes between the years of our respective observing runs.

2.2. *The Infrared Calcium Triplet*

Chromospheric activity can be identified also in lines which are too narrow to isolate the chromospheric signature as an isolated emission. At least in active-chromosphere stars, the filling-in by an incipient emission shows up as a decreased depth of strong absorption lines, in particular in hydrogen Hα, and in the infrared Ca II triplet 849.8, 854.2, and 866.2 nm (e.g., Linsky et al. 1979a; Cayrel et al. 1983; Foing et al. 1989).

Foing et al. (1989) subtracted pairs of Ca II triplet spectra for stars with similar temperatures, but with different activity levels, finding very similar parameters for β Hyi and the Sun. Considering the lower metal abundance in β Hyi (and thus the smaller depths expected in photospheric absorption lines), this could be taken to indicate a somewhat smaller chromospheric contribution in β Hyi.

2.3. *Hydrogen and Helium Lines*

2.3.1. *Balmer α*

In a survey of southern late-type stars, Zarro & Rodgers (1983) and Zarro (1983) studied Hα also in β Hyi and moonlight. They remark that stars with weak Ca II K emission, e.g., β Hyi, exhibit "bell-shaped" Hα absorption cores, whereas the more active dwarfs show peaked cores suggestive of emission components. Both the Hα residual flux and Ca II K emission strengths were found to be weaker in β Hyi than in integrated sunlight, thus adding another evidence for its low activity. Also Pasquini & Pallavicini (1991) measured the Hα "excess" flux of apparent chromospheric origin in G and K stars, finding a considerably lower value for β Hyi than the solar one.

Since, in solar-type stars, the Hα excitation is strongly influenced by Hβ and the background continuum, while its opacity is controlled by (nonlocal) photoionization, the Hα line may not carry direct information on the local chromospheric properties. Nevertheless, as shown by Cram & Mullan (1985), it still conveys information on chromospheric structure, complementary to that in collision-dominated lines.

2.3.2. *Lyman α*

In the Sun, Lyα is excited mostly by collisions, while Lyβ, Hα, and the Lyman continuum are controlled by the Lyα radiation field (Skumanich & Lites 1986). Lyα is thus primarily a chromospheric diagnostic which, due to the large abundance of hydrogen, is formed high in the chromosphere. We have measured the Lyα flux in β Hyi using the *IUE* satellite, and these data are discussed together with the rest of its far-ultraviolet spectrum in Paper III.

2.3.3. He I λ1083 nm *and* D_3 *lines*

The very high excitation triplet He I lines have excitation potentials of their lower levels $\chi = 19.73$ eV (1083.0 nm) and $\chi = 20.87$ eV (587.6 nm; D_3), respectively, and thus must be formed under rather different conditions than more ordinary chromospheric lines. On the Sun, D_3 and 1083 nm appear in absorption. In equivalent width, D_3 is typically a factor 10 weaker than λ1083 and largely coincides with active plage regions. The 1083 nm absorption is strongest above active regions, but very weak (even faintly in emission) in coronal holes.

The population of the lower states of these He I transitions in late-type stars is probably determined by recombination following photoionization of He I by X-rays shining down from a hot corona (Zirin 1975). In this case, the population levels (and the equivalent widths) should be roughly proportional to the coronal soft X-ray flux, making these He I lines diagnostics primarily of the corona, and less of the chromosphere. For further discussions, see Smith (1983), Wolff & Heasley (1984), and Avrett, Fontenla, & Loeser (1992).

The solar He I λ1083 nm absorption line undergoes great changes (a factor $\simeq 3$) during the solar activity cycle, but has a typical equivalent width of $\simeq 5$ pm (50 mÅ). Judging from the later discussion in paper III, the solar and β Hyi fluxes should not be drastically different in the far-UV region, and one could therefore expect the solar and β Hyi He I λ1083 lines to be of comparable strength. We are not aware of any high-resolution spectra of β Hyi in this infrared region, but this line should be observable with modern array detectors.

However, the nondetection of coronal X-ray flux from Arcturus (Ayres, Fleming, & Schmitt 1991), a star with variable 1083 nm He I emission, shows that (at least) in giant stars also other excitation mechanisms must be at work, possibly hydrodynamic shock waves.

The D_3 line may also be an indicator of coronal properties. A number of authors have studied D_3 in stars, and the survey made by Danks & Lambert (1985) included β Hyi. However, only an upper limit of $W < 0.2$ pm (2 mÅ) could be set for this He I 587.6 nm line. The solar value is about 10 times larger in active regions, but extremely small in the quiet Sun. Our attempts to estimate its strength in spectral atlases of integrated sunlight were not successful, due to severe contamination by telluric H_2O lines, which must be accurately

corrected for, before any reliable solar feature can be measured. In any case, the weakness of the D_3 feature in β Hyi is another indication of its low level of activity.

2.4. Mg II *h and k lines*

Similar to Ca II H and K, the lines of the Mg II resonance doublet *h* (280.27 nm) and *k* (279.55 nm) are collisionally excited and thermalized in the chromosphere, making them sensitive diagnostics for the structure of the upper photosphere, the temperature minimum, and the lower chromosphere. Since the cosmic abundance of magnesium is some 14 times that of calcium, and the Mg II *h* and *k* lines are intrinsically stronger, their chromospheric optical depths are normally at least one order of magnitude greater, and their level of formation correspondingly higher. Thus, the magnesium features reflect chromospheric properties at somewhat higher temperatures and greater atmospheric heights than the calcium lines. For cool stars, the lower flux level of the photospheric continuum in the ultraviolet, as compared to the Ca II H and K region in the violet, further increases the visibility of the chromospheric emission. However, in absolute flux units, the *h* and *k* emission cores are quite comparable to H & K: the apparent difference of the spectrum is mainly due to the enhanced contrast in the ultraviolet. The most extensive review of the Mg II doublet in stars is the monograph by Gurzadyan (1984).

However, this increased line strength also means a great sensitivity to interstellar absorption. While observed Ca II H & K lines usually are the true stellar profiles, the Mg II ones may be contaminated by interstellar and/or circumstellar components.

2.4.1. *Observations of* Mg II *h and k*

An extensive series of observations of Mg II in β Hyi was carried out from the *IUE* satellite during some 12 yr, which (together with some additional spectra recorded by others) yielded more than 100 high-resolution spectra of the Mg II region. These data were primarily collected to search for time variability (as discussed further in § 3.2 below) and were subject to an elaborate data processing as described in the Appendix.

Here, we show the 12 yr average of the Mg II profiles in Figure 2, also comparing to solar data. This β Hyi spectrum, being the average of about 100 well-exposed high-resolution *IUE* exposures, and processed with special techniques, is probably the highest quality spectrum of any object recorded with the *IUE* satellite. The comparison with integrated sunlight is with that spectrum of the Moon in the *IUE* data archive (LWR 9969), which was best exposed for the Mg II emission, here slightly noise-filtered.

The *IUE* wavelength scale was slightly corrected to match the solar atlas by Kohl, Parkinson, & Kurucz (1978). Since the *h* and *k* emissions appear at the edges of successive echelle orders, the exact pseudocontinuum shape in the reconstructed spectrum depends sensitively upon the precise blaze ("echelle ripple") correction applied. Following various tests, this was computed as in Allocchio, Morossi, & Vladilo (1984; after correcting their formula [4b] for the lack of a factor 100). The *IUE* spectral order 83 contains both the *h* and *k* lines. Mg II *h*

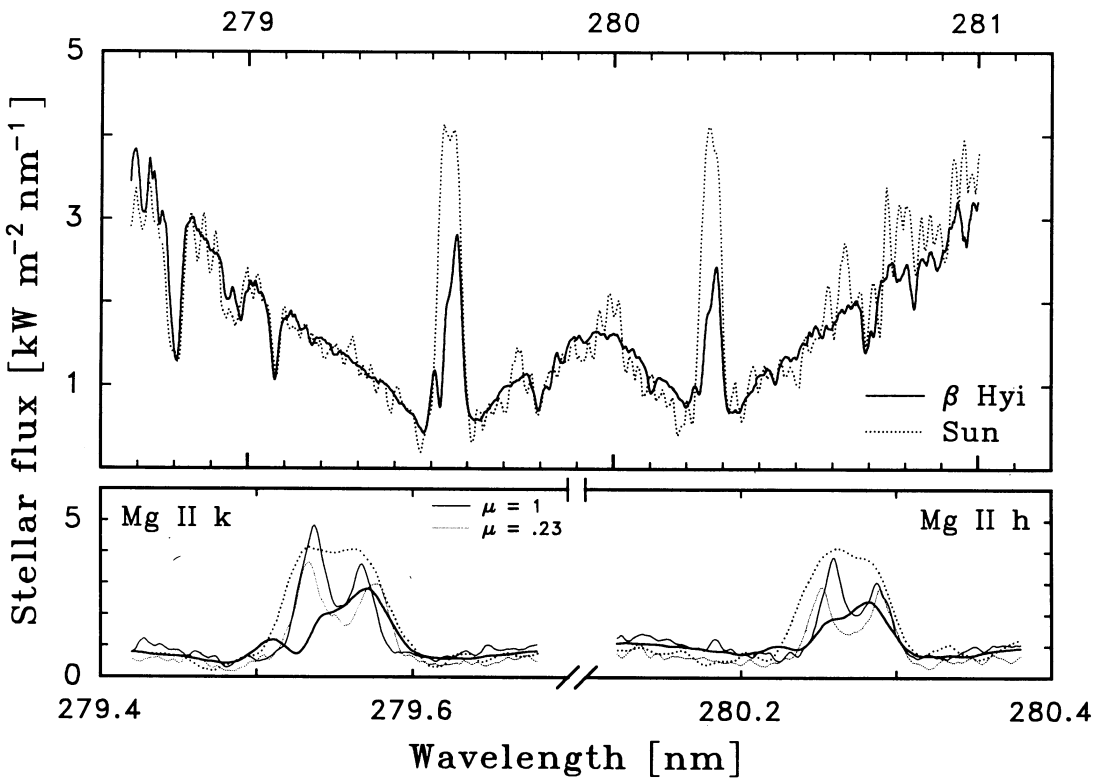

FIG. 2.—Line profiles for Mg II *h* and *k*, compared to solar data. For β Hyi, the average profile over 12 yr is shown (*bold*), while the dotted curve is the spectrum of integrated sunlight, as revealed by an *IUE* observation of the Moon with nominally identical instrumental settings. The expanded plots at bottom also compare with spatially resolved solar data with higher spectral resolution ($\lambda/\Delta\lambda \simeq 90{,}000$) for quiet regions at solar disk center ($\mu = \cos\theta = 1$; *thin solid*), and closer to the limb at $\mu = 0.23$ (*thin dotted*).

appears also in order 82, and following its blaze correction, its intensity was normalized to make the *h* emission agree in both orders, whereafter the overlapping order portions around the *h* line were averaged, and data from both orders merged.

2.4.2. *The Opposite Asymmetry in* Mg II *Emission*

Analogous to Ca II H and K, the Mg II *h* and *k* profiles show an emission weaker than in the Sun (Fig. 2). However, for Mg II the sense of asymmetry is *opposite* to that ordinarily seen in spatially resolved profiles on the Sun, i.e., the longward ("red") peak is the strongest, and there is a sharp absorption-type feature in the shortward flank of the emission peak.

These characteristics have been noticed by some authors, including Stencel et al. (1980) who noted the β Hyi profile as "peculiar" among several other cool stars. A more ordinary Mg II profile for another star classified as G2 IV–V (HD 67228) is in García-Alegre, Ponz, & Vázquez (1981). We now examine possible explanations for this discrepancy.

Attention has been drawn in the literature to stars whose emission features have such "discrepant asymmetries" in Ca II and Mg II. The origin might be connected to (greatly) different levels of line formation in outflowing atmospheres, or absorption effects in dense stellar winds (Mullan 1984, and references therein). However, while such effects may exist in luminous giants, they seem most unlikely in quiet solar-type stars. Alternatively, they could be due to interstellar absorption (Vladilo et al. 1987).

2.4.3. *Interstellar Absorption*

The Mg II *h* and *k* doublet is a sensitive probe for studying the interstellar medium, viewing these absorption lines against the continuum radiation from, e.g., early-type stars. However, as shown by Vladilo et al. (1985) and Molaro, Vladilo, & Beckman (1986), it is possible to study interstellar features in absorption against also chromospheric emissions. Of course, their complex shapes introduce the difficulty of determining which features are chromospheric, and which are interstellar.

Their studies include Mg II spectra also of β Hyi, and they interpret the blueshifted absorption seen in Figure 2 (for which they give a velocity of -23.5 km s^{-1} with respect to the stellar photosphere) as interstellar, and the redshifted feature at $+8$ km s^{-1} as chromospheric. The argument for the shortward feature being interstellar is that its velocity agrees with that expected from a uniform flow of the local interstellar medium, as measured in some other stars in the same part of the sky. The unknown strength of this (blueshifted) interstellar component makes it awkward to precisely deduce the intrinsic chromospheric profile, but it could explain the "inverse" Mg II asymmetries as caused by erosion by an interstellar component.

Vladilo et al. (1985) and Molaro et al. (1986) further deduce a Mg II column density toward β Hyi, which is clearly higher than for other stars at similar distances, indicating that β Hyi lies in a "high-density" part of the sky. For futher discussions of its position within the local interstellar cloud, see Bzowski (1988) and Génova et al. (1989, 1990).

There is no evidence for any interstellar calcium components in Figure 1. This need not be surprising since interstellar Ca II is much weaker than Mg II and not really expected to be visible.

Although one would ordinarily not expect so significant an interstellar absorption toward stars as close as β Hyi, it is also not surprising since the interstellar medium is highly inhomogeneous. Accepting this interpretation, we face a limitation in the possible modeling of the chromosphere using Mg II alone, since the intrinsic emission profile cannot be readily determined. However, it does not exclude searches for chromospheric variability, since there are no indications that the interstellar medium structure can change on our short observational time scales.

Measurements with very high spectral resolution will ultimately be required to fully segregate the probable interstellar components in β Hyi, and thus to finally settle the question of the origins of the Mg II signature. Analogous problems (and possibilities) are present in Lyα (although with the additional task of segregating the geocoronal emission).

2.4.4. *Observations by Other Authors*

Mg II profiles of β Hyi have been published by different authors. Indeed, several have used our *IUE* observations (which have been available in the *IUE* archive during the several years of our variability search), extracted using various data processing routines. Stencel et al. (1980) and Franco et al. (1984) deduced a series of line parameters. Moreover, an earlier observation from the *Copernicus* satellite is available (Weiler & Oegerle 1979).

2.4.5. *Solar* Mg II

Not many high-resolution observations exist of Mg II in the spectrum of the Sun seen as a star, although some *IUE* exposures of the Moon have been made. We now compare our β Hyi data to such observations of the Moon, as well as spectra of spatially resolved solar features. (Originally, we had also planned to follow the solar cycle in Mg II of moonlight. Unfortunately, in the early days of the *IUE* project, certain technical problems made this difficult, and when the capability later arrived, revealing a high cost in observing time, we set our priorities on β Hyi only.)

Only a few suitably exposed high-resolution spectra of the Moon exist in the *IUE* archive, and among these we selected LWR 9969; Figure 2. This 8.5 minute exposure was recorded on 1981 February 21, not long after the sunspot maximum in 1979/1980. The exposure was made with nominally the same settings, and with the same LWR detector as used for our β Hyi spectra. Even so, possible systematic differences due to instrumental effects cannot be excluded. The effective entrance apertures (and the ensuing spectral resolutions) could be slightly different, if moonlight uniformly fills the entire spectrograph aperture in a different manner than the peaked optical image of a star. However, the small spectrograph aperture used here ($\varnothing$ = nominally 3″; actually 4.″0 for the LWR camera), as filled by moonlight, is quite comparable to the size of the optical image of a star falling onto the large aperture, and this should not introduce any significant differences in spectral appearance.

The expanded plots at bottom also compare with spatially resolved solar data with higher spectral resolution ($\lambda/\Delta\lambda \simeq$ 90,000). These data are (slightly noise-filtered) absolute spectral intensities from Kohl & Parkinson (1976; also presented in the atlas by Kohl et al. 1978). They refer to *quiet regions* at solar disk center ($\mu = \cos\theta = 1$; *thin solid*), and closer to the limb at $\mu = 0.23 \pm 0.04$ (*thin dotted*). The absolute flux scale in Figure 2 was obtained by normalizing the *IUE* spectra to a (weighted) average of the $\mu = 1$ and $\mu = 0.23$ solar data in the line wings. Although the effective temperatures of β Hyi and the Sun are similar, one cannot exclude some systematic effects due to their

slightly different metallicities. Nevertheless, the resulting flux scale agrees closely (within $\simeq 20\%$) with that obtained by combining the *IUE* instrumental calibration with stellar flux scaling from apparent stellar diameter and photometric color (Stencel et al. 1980).

The spectrum of integrated sunlight is expected to be some sort of weighted average of the disk center and near-limb profiles, augmented in intensity due to contributions from active regions and other features, most of which show double-peaked emission (e.g., Lemaire & Skumanich 1973). However, as seen in Figure 2, the *h* and *k* emission peaks in sunlight have remarkably flat cores, considering the pronounced asymmetries in the spatially resolved profiles. We are not aware of previously published Mg II spectra of integrated sunlight in a high-resolution format, and to verify the reality of this phenomenon, other spectra of moonlight from the *IUE* archive were examined. However, all these (LWR 8627, LWR 9960, LWR 9968), recorded during different years, show the same type of feature (within the expected noise levels), and in both spectral orders available.

The subtle differences that may exist between the spectra of integrated sunlight and moonlight (Lind & Dravins 1980) are much too small to explain the single-peaked profiles in Figure 2. However, these can be understood if the spectral resolution was about a factor of 2 lower than in the stellar spectra. Although such a difference appears greater than could be expected, and should also have revealed itself as increased absorption-line widths, at this time we are unable to offer any better explanation.

The observed Mg II emission in β Hyi is significantly weaker than that in the Sun, and also lower than in α Cen A. As discussed above, any more detailed comparison is constrained by the ignorance of the precise amounts of interstellar absorption. In addition, one cannot exclude the possibility that some part of the absorption components represent the development of a cool stellar wind like that seen clearly in low-mass K giants, an evolutionary stage toward which β Hyi presently is heading.

Ultraviolet spectra of "solar spectral analogs" are discussed by Altamore et al. (1990), who study also Mg II *h* and *k* in a sample that includes β Hyi and moonlight.

2.5. *Chromospheric Emission Dependence on Age*

Stellar activity, as well as rotation, statistically decreases with increasing stellar age. However, whether the fundamental correlation is between activity and age, or between activity and some rotation-related parameter, is less obvious.

Stępień (1989) compiled data from various sources to arrive at a dependence for the excess calcium emission $\Delta F_{\mathrm{Ca\,II}}$ above the "basal" value, which for older stars takes the form $\Delta(\log \Delta F_{\mathrm{Ca\,II}}) = -0.5\Delta \log t$. For a doubling of the present solar age, this implies a Ca II emission decrease by 40% from the present, consistent with what is seen in β Hyi. Rather similar relations were found by Barry, Cromwell, & Hege (1987) in an analysis of H and K in eight clusters of widely different ages. In a classical paper, Skumanich (1972) found that the data points available at that time were consistent with a decay $\propto t^{-1/2}$ for both Ca II K emission, and stellar rotation.

The decrease of Mg II emission largely follows that of Ca II (Simon, Herbig, & Boesgaard 1985). However, the estimate of functional forms for its decay is limited by the scarcity of data for stars with well-determined ages, as well as the unknown effects of interstellar absorption.

2.5.1. *Time Evolution of Stellar Rotation*

The Sun is continuously losing rotational angular momentum through its magnetic stellar wind. The relation between rotation and age t on the main sequence is consistent with $\langle v \sin i \rangle \propto t^{-1/2}$, except for very young stars (Soderblom 1983). At the time of main-sequence arrival, the Sun can be expected to have rotated at roughly 10 times its present rate, which rapidly declined by perhaps a factor 3 during the first billion years or so. An extrapolation suggests that the further solar rotational decline in the next 5 billion yr should be a factor $\simeq 1.5$, i.e., extending the rotational period from the present 27 to perhaps 40 days. Our best estimate of $v \sin i$ for β Hyi of 2 ± 1 km s^{-1} (§ 2.1.5 in Paper I) is fully consistent with such a period.

3. CHROMOSPHERIC VARIABILITY

Solar-type variability occurs on widely different time scales: (*a*) over many years, due to the modulation of surface activity during a magnetic activity cycle; (*b*) over weeks and months, related to the rotation of active regions onto and away from the visible hemisphere; (*c*) over hours and days, mirroring the emergence and growth of active regions; and (*d*) over minutes or less, during the impulsive brightening of flares.

3.1. *Time Variability of Emission Lines*

Does the emission in β Hyi merely show a basal chromospheric component, or are there variable (magnetic) components on top of this? And on which time scales is there detectable variability?

Hitherto, activity cycles in solar-type stars have been detected in the Ca II emission *flux* only. In the case of a low-activity star such as β Hyi, where this emission is barely detectable even in high-resolution spectra (Fig. 1), some other approach is required, especially if searching also for *line profile* variability. For this purpose, a Mg II *h* and *k* survey was carried out using the *IUE* satellite. The much greater contrast in the Mg II profiles (Fig. 2) eliminates many of the observational problems of Ca II, while introducing others, such as the technical one of running long-term programs from spacecraft, and the astrophysical one of the great sensitivity of Mg II lines also to other phenomena, such as interstellar absorption.

3.1.1. *Monitoring β Hyi from IUE*

A search for Mg II variability was thus carried out from *IUE*, spanning a period of about 12 yr. Thanks to its position close to the south celestial pole ($\delta = -77°$), β Hyi escaped all geometrical constraints for the *IUE* spacecraft (which restrict pointing its telescope toward the proximity of the Sun, Earth, Moon, etc.) and thus could be observed at any time. Only several years into the *IUE* project did additional constraints appear, connected with the required sunlight illumination angle of the (now degraded) solar panels, which began to limit the observability of β Hyi.

Between 1978 and 1989, 101 high-resolution spectra were recorded on 34 different observing days, including also some spectra in the *IUE* data archive obtained by others (Table 1). Of these, 99 were recorded with the LWR (Long-Wavelength Redundant) camera; 88 specifically for this program, and the remainder for other programs or for calibration purposes. There also exist two images recorded with the LWP camera (which, however, would have required a separate photometric analysis, and are not used here). Finally, there is the earlier observation from *Copernicus*.

TABLE 1

LIST OF ALL HIGH-DISPERSION *IUE* SPECTRAL IMAGES OF β HYDRI EXPOSED FOR THE Mg II *h* AND *k* LINES

IUE Image number	Date (y-m-d)	Apert.	Exp. [min.]
LWR 1593	78-06-02	S	15
LWR 1863	78-07-20	S	16
LWR 2192	78-08-27	S	13
LWR 2610	78-10-15	S	30
LWR 2811	78-11-03	S	15
LWR 2812	78-11-03	S	15
LWR 2813	78-11-03	S	15
LWR 2833	78-11-05	S	15
LWR 2834	78-11-05	S	15
LWR 3700	79-02-07	L	8.5
LWR 4714	79-06-06	L	20
LWR 4794	79-06-16	L	7.5
LWR 4795	79-06-17	L	7.5
LWR 4796	79-06-17	L	10
LWR 4797	79-06-17	L	10
LWR 4798	79-06-17	L	10
LWR 4807	79-06-18	L	10
LWR 4808	79-06-18	L	10
LWR 4809	79-06-18	L	7
LWR 4810	79-06-18	L	7.5
LWR 5309	79-08-09	L	25
LWR 6296	79-12-03	L	8
LWR 6426	79-12-18	L	15
LWR 6853	80-02-04	L	10
LWR 6854	80-02-04	L	10
LWR 6855	80-02-04	L	10
LWR 6856	80-02-04	L	15
LWR 6857	80-02-04	L	15
LWR 7894	80-05-30	L	15
LWR 7895	80-05-30	L	15
LWR 7896	80-05-30	L	15
LWR 7897	80-05-30	L	15
LWR 7898	80-05-30	L	15
LWR 9684	81-01-10	L	15
LWR 9685	81-01-10	L	15
LWR 9686	81-01-10	L	15
LWR 9687	81-01-10	L	15
LWR 9688	81-01-10	L	15
LWR 10237	81-03-29	L	15
LWR 10238	81-03-29	L	15
LWR 10239	81-03-29	L	15
LWR 10605	81-05-14	L	7
LWR 11943	81-11-08	L	15
LWR 11944	81-11-08	L	15
LWR 11945	81-11-08	L	15
LWR 11946	81-11-08	L	15
LWR 12552	82-02-11	L	15
LWR 12553	82-02-11	L	15
LWR 12554	82-02-11	L	15
LWR 12555	82-02-11	L	15
LWR 12556	82-02-11	L	15
LWR 12557	82-02-11	L	15
LWR 12558	82-02-11	L	15
LWR 12559	82-02-11	L	15
LWR 12570	82-02-12	L	17
LWR 12571	82-02-13	L	30
LWR 12916	82-03-31	L	6.5
LWR 13730	82-07-20	L	7
LWR 13731	82-07-20	L	15
LWR 13732	82-07-21	L	15
LWR 13733	82-07-21	L	15
LWR 13734	82-07-21	L	15
LWR 14929	82-12-27	L	15
LWR 14930	82-12-27	L	15
LWR 14931	82-12-27	L	15
LWR 14932	82-12-27	L	15
LWR 14933	82-12-27	L	15
LWR 15382	83-02-27	L	15
LWR 15383	83-02-27	L	15
LWR 15384	83-02-27	L	15
LWR 15385	83-02-27	L	15
LWR 15386	83-02-27	L	15
LWR 15437	83-03-07	L	6.5
LWR 16698	83-08-29	L	15
LWR 16699	83-08-29	L	15
LWR 16700	83-08-29	L	6.5
LWR 16701	83-08-29	L	15
LWR 16702	83-08-29	L	15
LWP 4915	84-12-03	L	8
LWR 17575	85-01-02	L	15
LWR 17576	85-01-02	L	15
LWR 17577	85-01-02	L	15
LWR 17578	85-01-02	L	15
LWP 6404	85-07-15	L	15
LWR 17876	86-04-01	L	20.5
LWR 17877	86-04-01	L	20.5
LWR 17878	86-04-01	L	20.5
LWR 17879	86-04-01	L	20.5
LWR 17924	86-07-08	L	20.5
LWR 17925	86-07-08	L	20.5
LWR 17926	86-07-08	L	20.5
LWR 18009	86-12-01	L	20.5
LWR 18010	86-12-01	L	20.5
LWR 18011	86-12-01	L	20.5
LWR 18012	86-12-01	L	20.5
LWR 18335	89-10-30	L	21
LWR 18336	89-10-30	L	21
LWR 18337	89-10-30	L	21
LWR 18338	89-10-30	L	21
LWR 18339	89-10-30	L	21
LWR 18340	89-10-30	L	21

[a] The spectrometer aperture used (small or large) is indicated, as well as the exposure time.

An effort was made to keep the observing material as homogeneous as possible, and the same LWR detector was continued to be used with its original readout procedures, even after these had been changed and the detector itself replaced by LWP as the standard. For example, at some time a certain type of transient data readout noise, affecting a small part of the image started to become common ("microphonics"). Although this was empirically found to be largely avoidable by using a certain detector heatup procedure prior to readout, we made an effort *not* to use this procedure (despite the increased risk of losing data), not being convinced that it would not affect the photometric calibration. After 1986, the standard exposure time had to be increased from 15 to 21 minutes, to retain the same exposure level on the detector, after technical problems necessitated a decrease of its voltage level and ensuing sensitivity. This exposure level was optimized for the chromospheric emission and the central parts of the Mg II absorption lines; the spectrum outside the region shown in Figure 2 became overexposed. While occasional data disturbances may impair parts of the spectra, data from all LWR images could be utilized.

3.1.2. *The Lund Procedure for IUE Spectral Image Processing*

The observed Mg II changes in β Hyi are small and comparable in magnitude to the inaccuracies of the standard *IUE* data reduction software. Numerous modifications to the latter during the course of the *IUE* mission further complicate the comparison of data from different epochs. To enable a study of stellar variability required a careful reexamination of the entire procedure for the processing of the *IUE* spectral images, and the subsequent extraction of the spectra. An unexpected result was that much of what previously was believed to be noise in the spectral images instead was found to be a fixed pattern of small-scale sensitivity variations across the detector surface, remaining constant over years. Once the geometric correction of the *IUE* spectral images could be attained to within a fraction of a pixel of the corresponding calibration images (not achieved by standard software), a significant noise source could be removed, and the signal-to-noise ratios improved to reveal the astrophysical variability.

Methods for the optimum processing of *IUE* data were thus developed which, in addition, incorporate some lesser improvements already applied elsewhere, e.g., in a better treatment of the interorder background, in the elimination of data disturbances, in the use of optimized extraction slits, etc. Our data were processed with these state-of-the-art methods and thus contain substantially less noise than previous spectra extracted from the same observations. Initially developed in Lund for this β Hyi project (Linde & Dravins 1988, 1990), these procedures have now been adopted by NASA and ESA as a cornerstone in the new software to be used for the reprocessing of the entire *IUE* data archive. An overview of these methods is presented in the Appendix.

3.2. Mg II *h and k Variability in* β *Hyi*

3.2.1. *Changes in h and k Fluxes*

Figure 3 shows the time evolution of the Mg II *h* and *k* emission *fluxes*, measured against an adjacent spectrum portion in the photospheric Mg II line wing. These flux data are similar in character to the Ca II K narrow-band photometer index recorded for many other stars at the Mount Wilson Observatory in monitoring chromospheric variability. Since there is very little photospheric background, and the contrast

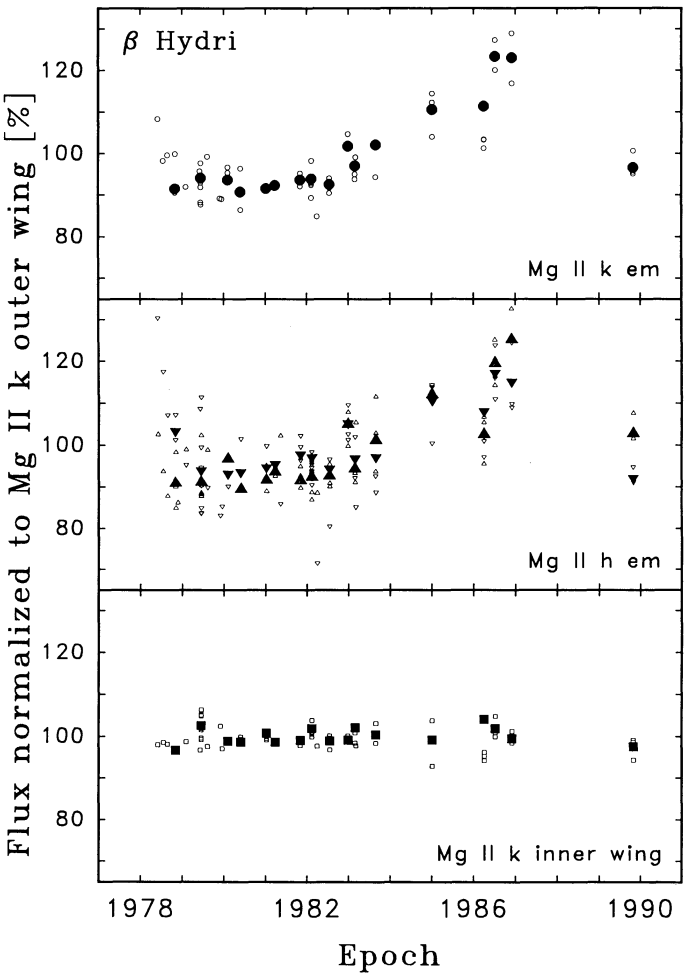

FIG. 3.—Long-term changes in Mg II *h* and *k* emission *fluxes* in β Hyi. At top are the equivalent widths of the *k* emission, at center those of *h*, and at bottom the inner *k* absorption line wing. Large symbols show high-quality data from epochs, when several *IUE* exposures were recorded. The *k* line appears in one spectral order only, but the *h* line was measured in both echelle order No. 83 (*top-down triangles*) and No. 82 (*top-up*). The variations are limited to the emissions proper, and there are no significant changes in the inner *k* line wing. The variability suggests an activity cycle with a period in the range $\simeq$15–18 yr.

in Mg II is much higher, any chromospheric emission changes should appear with much greater amplitude than in such Ca II K measurements.

For data from those 17 months, when sequences of at least three *IUE* exposures had been recorded (five on the average; Table 1), higher quality composite spectra could be computed and these data are shown as large filled symbols. In addition, data from that *subset* of individual exposures are shown, whose spectra contained no apparent data disturbances for *either* the chromospheric emission or the reference level (*small open symbols*). Besides filling in data for some additional epochs, these points serve to illustrate the typical spread of data.

The Mg II *h* line appears in echelle spectral order No. 82 (and marginally in No. 83), and the *k* line in No. 83. The *k* emission flux (integrated over a wavelength interval equal to that between the intensity minima on both sides of the emission for the average spectrum in Fig. 2) was normalized to the interval 278.81–279.08 nm (between the two distinct Fe I absorption lines) in the shortward outer *k* wing. This was the best

"pseudocontinuum" available; the only close to the emissions of interest, and not overexposed on the detector. This "pseudocontinuum" is thus assumed constant. The contribution from the underlying photospheric line can be estimated to perhaps one-third or a quarter of the flux signal, but no subtraction of it was made. The same interval was used to normalize the *h* flux, as measured near the end of the same spectral order No. 83 (*top-down triangles*). The *h* line also appears in spectral order No. 82, and those fluxes were normalized to an interval $\simeq$0.3–0.6 nm from line center in the longward *h* wing in that spectral order (*top-up*). Although the *h* data are noisier, they serve both to verify the trends seen in *k*, and to illustrate the consistency of data from different spectral orders (which fall on entirely different parts of the *IUE* detector). At bottom is shown the behavior of the shortward *inner* wing of the *k* photospheric absorption line, covering the wavelength interval from the shortward intensity minimum just outside the emission, to 279.08 nm, normalized to the outer wing as above for order No. 83. The average for all measurements of each parameter was set to 100%.

Figure 3 shows how the Mg II emission in β Hyi changes in a gradual and systematic manner, completely consistent for all three independent measurements (*k*, and *h* in its two orders). These variations are limited to the emission proper, and there are no significant variations in the inner *k* line wing (further demonstrating the reality of the emission changes). During these 12 yr there has been both one activity minimum (around 1980) and one maximum (1986), suggesting an activity cycle with a period in the range of $\simeq$15–18 yr, i.e., somewhat longer than the solar one. For the 11 yr solar cycle, the time from minimum to maximum is typically some 4 yr (and $\simeq$7 yr from maximum to minimum). Assuming the same asymmetry in the β Hyi cycle would imply a factor $\simeq$1.5 relative to the Sun: about 17 yr. The peak-to-peak amplitude in the emission fluxes is about 30%, with notably similar amplitudes in *h* and *k*.

3.2.2. *Correspondence to the Mount Wilson* Ca II H *and* K *Flux Index*

Extensive surveys of long-term variability in stars have been carried out at the Mount Wilson Observatory. The photometric flux is measured in a narrow band around the Ca II H and K line centers, normalized to the adjacent (pseudo)continuum. For the Sun, such an activity index mainly gives a measure of the active region plage area coverage and brightness. Results are presented by Wilson (1978) and reviewed by Baliunas & Vaughan (1985), while Dravins (1990) discusses different types of known and expected activity cycles in the Sun and stars.

There seems to be a systematic trend in that the most active stars show more irregular fluctuations and that regular activity cycles appear mainly in stars of moderate activity levels. Our β Hyi results confirm this trend of very low activity being accompanied by smooth and gradual changes. Among those early G main-sequence stars in the Mount Wilson survey which have "weak emission," only about one-half show variability above the noise level, which is a few percent in the H and K index (Baliunas & Vaughan 1985).

Beta Hyi is too far south in the sky to be visible from Mount Wilson in California, but we have computed the expected variability in the Mount Wilson Ca H and K index. The instrumental profile of the current Mount Wilson spectrophotometer is triangular in shape, centered on the K and H line cores, and with full width at half-maximum = 0.109 nm (Duncan et al. 1991).

To compute the effect in the H and K index, we must first estimate which parts of the Ca II profiles take part in the changes observed in Mg II. Many attempts have been made in the literature to separate the chromospheric emission component from a "photospheric" one which could arise in a (hypothetical?) "quiet" atmosphere. Ideally, one would have liked to compare to the spectrum of an otherwise identical star, but with "zero" activity, or to use some ab initio modeling of chromospheric inhomogeneities and the resulting line profiles. Since such options are not yet available, we resort to some simpler definition. We will use that of the apparent emission features above a smooth absorption (extrapolated between the absorption line flanks and extending to the observed line bottom). This approximation holds for a two-component chromosphere, where emission from varying active region areas add to a "basal" profile, but is not far from what actually is observed for the Sun (White & Livingston 1981; Keil & Worden 1984).

We thus assume that the variations in Ca II H and K follow those in Mg II *h* and *k*, i.e., are confined to the emission proper and do not extend to the inner photospheric line wings (Fig. 3). The flux of the Ca II spectrum (Fig. 1) inside the Mount Wilson instrumental profile is then computed. Of that signal, the Ca II K and H emissions above the apparently smooth photospheric line background contribute about 2% of the signal, the remaining 98% coming from the (photospheric) inner line wings. The contribution from instrumental scattered light appears to be quite comparable for the Mount Wilson instrument (Duncan et al. 1991) and the present measurements.

In contrast, the underlying photospheric contribution to our Mg II flux measure is only about one-third or a quarter of the total (cf. Fig. 2). The observed Mg II flux variability of $\simeq$30% then implies some 40% change in the chromospheric emission proper, translating to an increase of the chromospheric K emission signal to $\simeq$2.8% of the total, and thus a total peak-to-peak amplitude during the stellar activity cycle of less than 1%!

An undetermined effect remains concerning the possible filling-in of the absorption line core and inner wings. Although no variability was observed in the Mg II inner wings (Fig. 3), such might conceivably be present in Ca II, which forms at somewhat different atmospheric heights. Even if such effects could somewhat increase the above figure of $\lesssim$1%, even a factor of 2 would be below the typical Mount Wilson noise level, indicating that the cycle in β Hyi has the lowest amplitude so far detected in any star. (In hindsight, it also justifies our decision to search for feeble activity changes in Mg II rather than in Ca II.

3.2.3. *The Significance of the Cycle in* β *Hydri*

Although our 12 yr of watching β Hyi feels to have been a long time, it is still very much shorter than ideally needed to understand long-term changes in stellar activity. What significance can then be ascribed to these years of data?

Perhaps the best guidance is obtained from comparing with simulated observations of the Sun over its past activity cycles. Gilliland & Baliunas (1987) subdivided the historical sunspot record into blocks of 12 or 18 yr, to see how well the 11 yr cycle could be identified. For stars of an activity level typical of the Mount Wilson survey, they find that the dominant noise source is undersampled rotational modulation of stochastically distributed active regions. In the 18 yr samples, the correct cycle period is identified in most cases, but the failure

rate increases for the shorter 12 yr blocks. Although, over the past hundred years, the solar cycle has been 11 yr on the average, the duration of individual cycles varies between about 7 and 17 yr, and the cycle amplitudes also vary.

Such discussions demonstrate the impossibility to reach irrevocable conclusions on long-term changes from our finite data series (even if it had been several years longer). Nevertheless, the smooth character of the variability in β Hyi strongly suggests an activity cycle as its cause (as opposed to, e.g., rotational modulation, emerging active regions or flaring activity). The smoothness of variations further suggests that noise sources pertaining to individual active regions are less significant than in more active stars. The cycle in β Hyi appears to be longer than the solar one by a factor of perhaps 1.5, a factor quite similar to the ratio of stellar radii and also their probable ratio of rotation periods.

3.2.4. Mg II *h and k Profile Changes*

Data from those 17 months, when sequences of at least three *IUE* exposures were recorded (cf. Table 1) permitted the computation of averaged composite spectra whose noise level is low enough to permit studies not only of changes in the flux but also in spectral line *profiles*. This long- and intermediate-term time variability of Mg II *h* and *k* profiles in β Hyi is shown in Figures 4*a* and 4*b*. The projection of the data surfaces there illustrates the slight decrease of activity for a few years after 1978, followed by the buildup to a maximum in 1986. The data strip in front marks the average for the full span of observations. Increased intensity is marked also by increased shading on the data surface. Data beyond the activity maximum are largely hidden in this projection, but the 1989 October profiles are very similar to the global averages. The corresponding *fluxes* for these 17 epochs were shown with the larger symbols in Figure 3.

Among ordinary stars, these data appear to represent the first detection of chromospheric variability suggestive of an activity cycle, seen in line *profiles* (and not merely fluxes). The profile changes from year to year are remarkably gradual (but systematic), possibly suggesting a smooth reorganization of the chromospheric structure rather than the sudden appearance of a limited number of active regions.

3.2.5. *Characteristics of Profile Variability*

Representative line profile changes during the period 1977–1989 are shown in Figure 5. Mg II *h* and *k* profiles are averaged during one calendar year, and shown at 3 yr intervals. Superposed dashed lines show the average of all spectra from the entire 1978–1989 *IUE* observing period. The changes at the activity maximum in 1986 are suggestive of a more structured profile developing. Assuming that the interstellar feature largely has eroded the shortward part of the shortward emission peak, one can envision that a more pronounced double-peaked emission was being produced at that time.

The Mg II *k* profile from 1977 in Figure 5*a* predates *IUE* and is the scan from *Copernicus* (Weiler & Oegerle 1979). Beta Hyi was observed as a "target of opportunity" during the dead time between spacecraft slews on 1977 April 28 (W. R. Oegerle, private communication). That scan did not extend into the line wings, precluding any "pseudocontinuum" normalization. Instead, the emission profile is here normalized to the *IUE* average. Although these measurements had a moderate resolution (0.05 nm) and are rather noisy, they do provide a data point about a year prior to the launch of *IUE*, illustrating the absence of any major line changes since that epoch also.

While Figure 5*a* showed the profiles at 3 yr intervals, Figure 5*b* gives their intensity *differences* relative to the 1978–1989 average. Changes in the weaker *h* line follow those in *k*, albeit with lower amplitude. Of particular interest is the "excess" emission at the epoch of activity maximum in 1986. Besides the suggestive development of an emission peak with a more complex structure, the apparent interstellar absorption feature is seen superposed on the shortward wing of the "excess" emission flux in both *h* and *k*. This supports the interstellar interpretation for the origin of the asymmetry in the Mg II emission (§ 2.4.3), since any additional flux emerging from the chromosphere must traverse the same interstellar clouds.

Once future high-resolution observations will have settled the question of the number, strength, and wavelength positions of interstellar components toward β Hyi, one should be able to interpret the ratio between *h* and *k* changes seen in Figure 5*b* in terms of, e.g., optically thick or thin emission. However, at the present time the unknown character of interstellar absorption makes this rather awkward to evaluate.

3.2.6. *Variability Studies by Other Authors*

Crivellari et al. (1983) used *IUE* data spanning some 4 yr to search for Mg II variability in different stars, including β Hyi (using both their own and our observations). Their results were negative: no variation in excess of their sensitivity limit of 15% could be seen. In a continued analysis of basically the same data, Franco et al. (1984) decreased the noise level by improving the spectrum extraction. While they concluded that the lines are constant within an error limit of 8%, they remark that the ensemble of β Hyi spectra hints at variability at levels just below the nominal noise level.

As discussed further in the Appendix, the certain detection of feeble variability, requires *both* improved *IUE* data reduction techniques *and* the averaging of several spectra to depress the noise. (For example, each of the *IUE* profiles in Fig. 5 represents the average of about 10 exposures.) Also, these previous studies suffered bad luck in the sense that, during the first several years of *IUE* observations, β Hyi underwent only quite small variations (Fig. 3).

3.3. *Solar Variability in* Ca II, Mg II, *and Other Lines*

We now review the variability of the Sun seen as a star, and compare to β Hyi.

3.3.1. *Solar Variability in* Ca II K

The solar-cycle variability of Ca II K emission in integrated sunlight has been studied by Sheeley (1967), White & Livingston (1981), Keil & Worden (1984), Sivaraman et al. (1987), White, Livingston, & Wallace (1987), and others. The K emission features above the apparent "basal" absorption line (as defined in § 3.2.2) increase by some 60%–70% between activity minimum and maximum, while the flux increase within the central 0.1 nm of the K line is $\simeq$15%–20%. The corresponding modulation of the Mount Wilson K index can be estimated to about half this value, consistent with the $\simeq$8% change measured in moonlight by Wilson (1978).

Since the line parameters appear to remain largely unchanged in quiet regions, it seems that these K line changes can be traced back to the additions of emission from active regions and from the magnetic network (Oranje 1983b; Skumanich et al. 1984; Schrijver 1988; Dobson et al. 1990).

3.3.2. *Solar Ultraviolet Variability*

The 11 yr cycle and 27 day rotation modulations of solar ultraviolet irradiance are being monitored by various space-

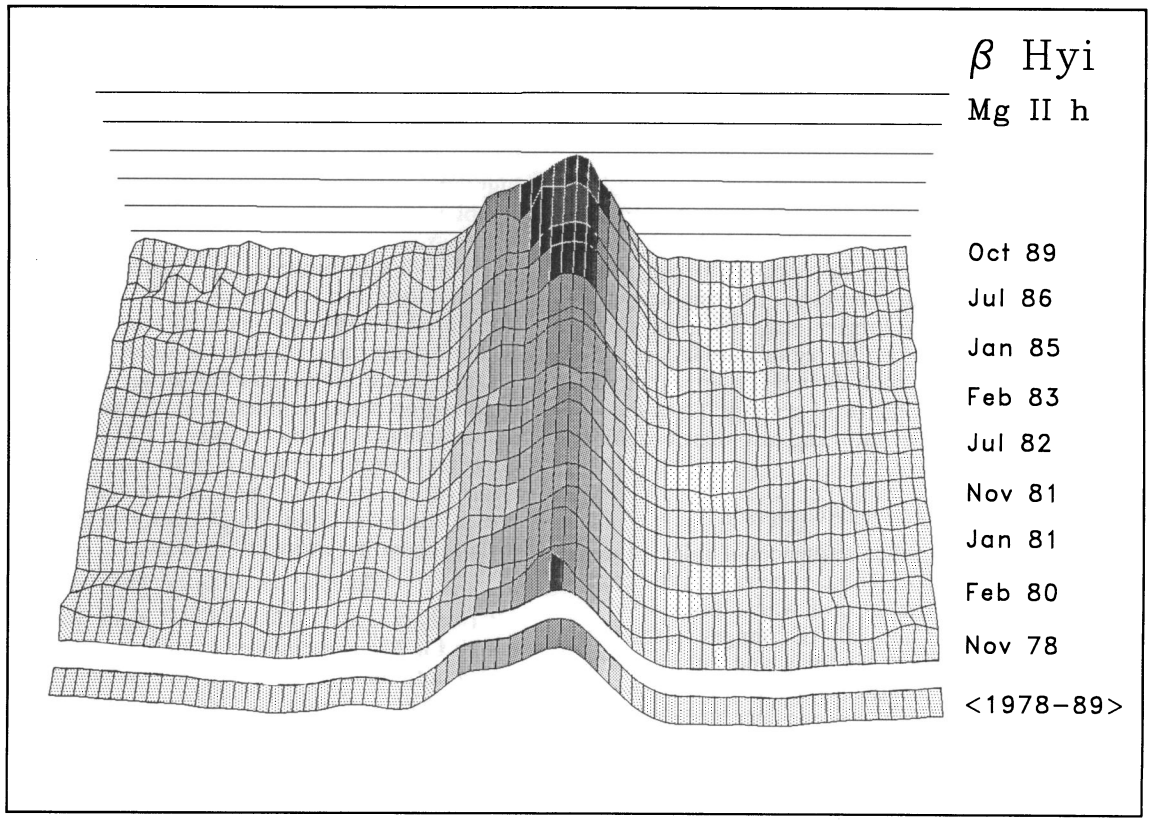

FIG. 4*a*

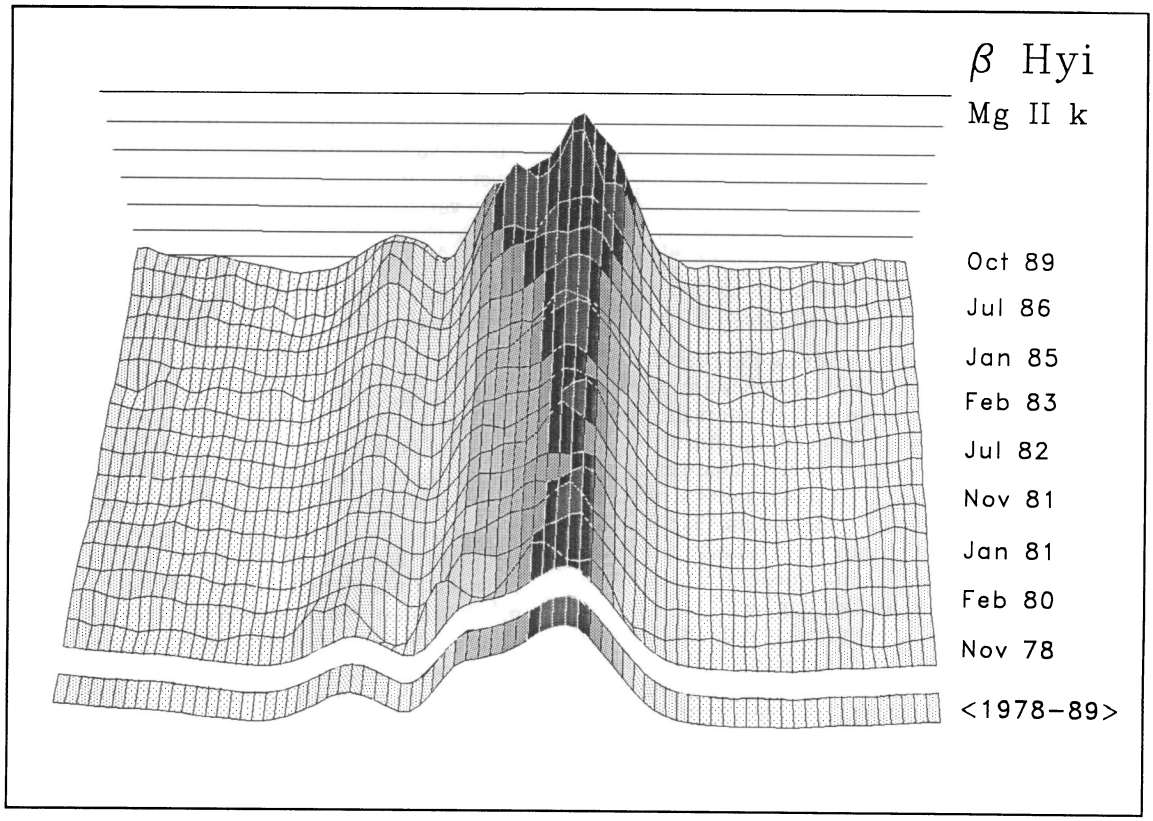

FIG. 4*b*

FIG. 4.—Long- and intermediate-term variability of Mg II *h* (*a*) and *k* (*b*) emission profiles in β Hyi. Data from the 17 best-observed epochs build up a surface of intensity versus wavelength. Every second epoch is labeled. The projection illustrates the slight decrease of activity for a few years after 1978, followed by the build-up to maximum in 1986. The data strip in front is the average profile. The changes over the years are remarkably gradual, and quite similar in both *h* and *k*.

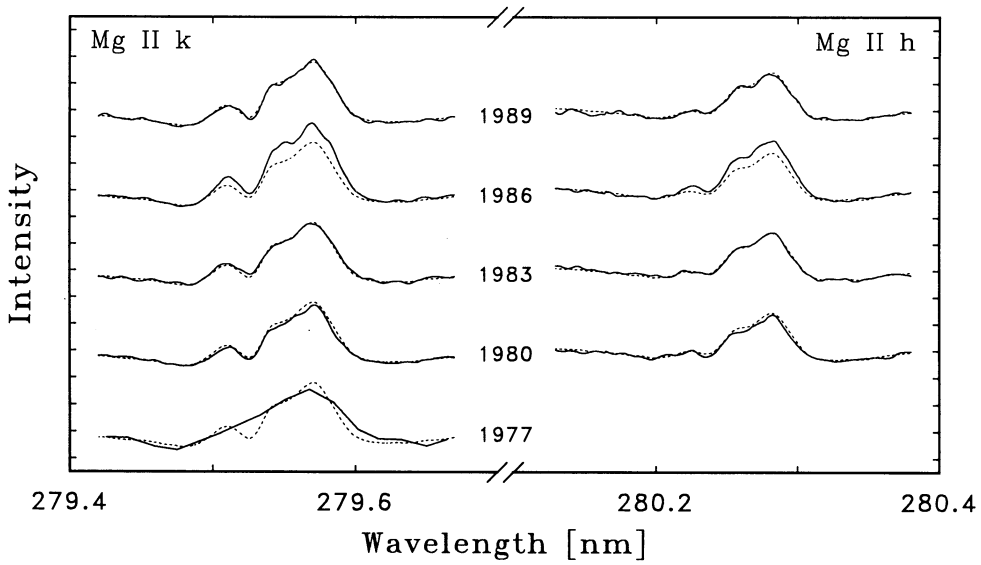

FIG. 5a

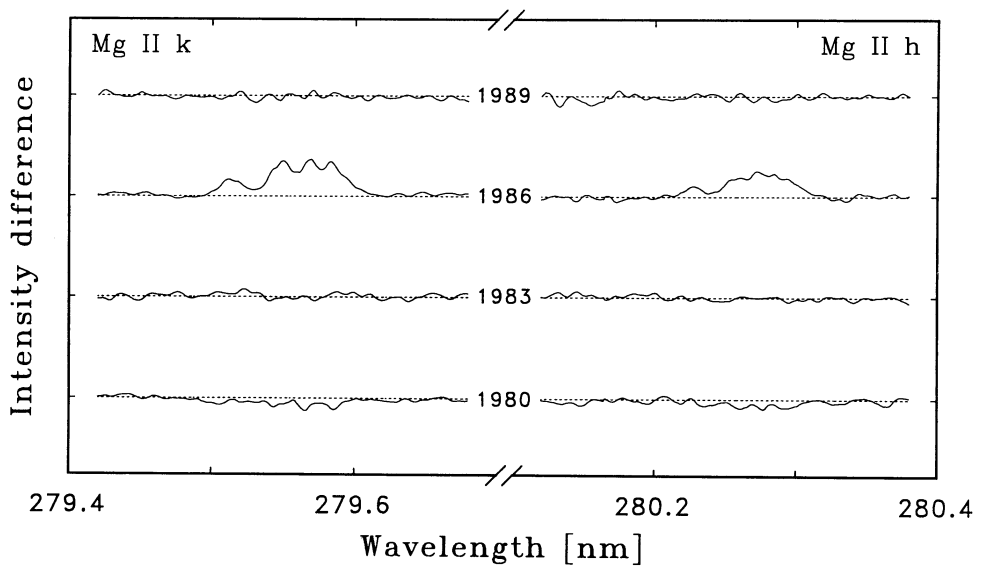

FIG. 5b

FIG. 5.—(*a*) Long-term variability of Mg II *h* and *k* profiles in β Hyi. Data averaged during one calendar year are shown at 3 yr intervals, illustrating representative changes during 1977–1989. Dashed lines show the average for the 1978–1989 *IUE* observing period. The 1977 profile is from *Copernicus*. (*b*) Characteristics of line profile variability in Mg II *h* and *k*. The intensity *difference* between 1 yr averaged profiles, and the average for the *IUE* observing period, are shown at 3 yr intervals. The weaker *h* line changes follow those in *k*. The apparent interstellar absorption feature in the shortward wing is seen superposed on the "excess" emission in both *h* and *k* at the 1986 activity maximum.

craft to study, in particular, how changes in the solar influx affect the terrestrial upper atmosphere. For reviews, see Lean (1987, 1990). A low spectral resolution (typically 1 nm) is often used, unfortunately insufficient to reveal any details of emission-line features. The variability increases toward shorter wavelengths and becomes especially strong in specific emission lines. For example, the activity cycle variation in Lyα is about a factor 2, and that of emission lines in the extreme ultraviolet a factor 5 or more.

The Mg II *h* and *k* lines show the (by far) largest modulation in their part of the spectrum (Heath & Schlesinger 1986). The measured amount naturally depends on the spectral resolution, i.e., whether the emission peaks are resolved or not. The solar-cycle amplitude in Mg II *h* and *k*, as deduced from a three-component model (quiet Sun, active network, and plage), fitted to data with 1 nm spectral passband, is $\simeq$20% (Lean 1984). Between different balloon flights, Hall (1983) observed a flux increase in the Mg II *h* and *k* emission cores (over 0.12 nm) by $\simeq$20% between 1977 (close to activity minimum) and 1981 (closer to maximum).

The widely different observational techniques make it nontrivial to directly relate the β Hyi variability to that of the Sun. However, the close correlation between Ca II and Mg II emission variations across the solar surface (e.g., Bonnet 1981) suggests that also temporal variations in Mg II should rather closely follow those in Ca II. While the solar Ca II K emission

features are some 60%–70% greater at activity maximum, the corresponding value for Mg II *h* and *k* in β Hyi is no more than $\simeq 40\%$ (§ 3.2.2).

Thus, not only is the activity *level* lower in β Hyi than in the Sun, but also its *relative* modulation during the activity cycle is smaller. If the chromospheric emission is half that of the Sun (Fig. 1), and its fractional modulation also perhaps one-half, then the amplitude in, e.g., the Mount Wilson K line index will be *one-quarter* of the solar one. Within the uncertainties, this seems consistent with the observed solar cycle amplitude in moonlight of $\simeq 8\%$ (Wilson 1978), and our estimate for β Hyi of $\simeq 1\%$ due to the emission peaks proper, *plus* any contributions due to changes in the line core and inner wings. These contributions from outside the emission peaks in β Hyi would also need to be on the order of 1%, in order for the K line index amplitude to be one-quarter of solar. However, more definitive statements must await a better understanding of the solar activity cycle in Mg II as well as the precise effects of interstellar absorption.

3.3.3. *Solar Variability in* He I λ1083 nm

Of all readily accessible spectral lines, the largest (known) amplitude during the solar cycle appears in the He I 1083.0 nm line, which varies by some 250%, is absorption strengthening with increasing activity (White & Livingston 1981; Harvey 1984; Lean 1990; Shcherbakov & Shcherbakova 1991).

As discussed in § 2.3.3, the λ1083 nm He I is a line of extremely high excitation potential, believed to be influenced by coronal soft X-rays, and with very little photospheric contribution. For further stellar studies, it could become the prime choice as a variability diagnostic for ground-based observations, as low-noise array detectors become available also in the infrared.

4. OUTLOOK FOR FUTURE STUDIES

Although a substantial observational effort was devoted to β Hyi, it is obvious that a single star is too small a sample to provide definite answers to subtle questions. Future studies will therefore require a larger statistical sample of evolved solar-type stars. However, at present, only some 10 old G subgiants of the β Hyi type are known with reasonably accurate ages. The brightest among those nonbinary stars that appears to be of comparable age as β Hyi, has apparent magnitude $m_v = 4.9$ (HR 4523, G5 V), a factor of 7 in apparent brightness. This relative faintness implies more demanding spectroscopic observations and in particular correlates with a more limited previous understanding of the stellar evolutionary status.

A promising future direction lies in utilizing space astrometry data from, e.g., the *HIPPARCOS* mission. It is currently measuring accurate distances (and thus luminosities) for many more stars, permitting evolutionary age determinations. With such data one can expect to identify a sample of perhaps 100 such evolved "Suns." While these may be rather fainter than β Hyi, it is hoped that they will still be bright enough for detailed spectroscopy with the several new large telescopes currently under construction.

This work was supported by the Swedish National Space Board and by the Swedish Natural Science Research Council. The development of *IUE* data analysis methods in Lund received support also from the European Space Agency. The initial *IUE* observing time was the result of a proposal submitted to ESRO already in 1972 (long before the actual launch of *IUE*) for a different program by a group also involving B. Gustafsson in Uppsala. At Uppsala we also thank B. Edvardsson for carrying out certain *IUE* observations at the Villafranca Satellite Tracking Station in Spain. Its staff offered most valuable help and advice during our more than 20 visits there and also made some of the actual observations. At Lund, H. Gleisner and U. Torkelsson contributed to parts of the data analysis. J. Beckman (Tenerife) clarified several questions on interstellar absorption, while J. L. Linsky (Boulder) and an anonymous referee gave many helpful comments on the manuscript.

APPENDIX

PRECISION PHOTOMETRY OF *IUE* SPECTRA

The spectrophotometric accuracy requirements in the study of Mg II variability required the development of algorithms for the *IUE* spectral image processing, superior to the standard software ("IUESIPS") ordinarily used. In this Appendix, we outline this procedure, developed for this β Hyi project at Lund Observatory, and which has since been adopted by the *IUE* project for the reprocessing of its entire data archive.

For a description of the *IUE* detector properties, their in-orbit performance, data quality limitations, common sources of noise, and standard procedures for spectral image processing, see Harris & Sonneborn (1987). Preliminary data reductions, using standard software, showed that typical Mg II *h* and *k* variations of stellar origin in β Hyi were no more than 10%–20%. A large literature exists on methods for analyzing *IUE* data, and several authors have confirmed the overall precision of data extracted with IUESIPS to lie around $\simeq 10\%$ (e.g., Ayres 1990), and thus better data reductions were essential to establish the chromospheric variability.

A1. PROBLEMS IN THE IUESIPS SOFTWARE

During the *IUE* project, the IUESIPS software has been "enhanced" many times, resulting in a heterogeneous treatment of data from different years. This alone makes it difficult to accurately compare data obtained at various times. Furthermore, it has long been known that improvements of IUESIPS are possible, but most such efforts have concerned better spectrum extraction, etc., from images whose geometrical and photometric processing still has been made in the standard way (e.g., Kinney, Bohlin, & Neill 1991). However, a more fundamental improvement is possible in the image-processing phase. The presence of nonrandom noise was identified already early in the *IUE* project, leading to the conclusion that spectrophotometric improvements must be possible if these noise sources could be found and removed (York & Jura 1982; Ayres 1990).

A1.1. *Fixed Pattern versus Random Noise*

The large quantity of β Hyi observations enable us to study variations in the LWR detector since 1978. In particular, a video display of a sequence of "raw" (i.e., unprocessed) exposures from different years reveals that most of the variation in the background (between spectral orders) is *not* random but rather forms a fixed pattern. Surprisingly, most of this pattern remains for images processed by IUESIPS, suggesting that its geometric transformation can be improved.

A1.2. *Improved Image Calibration*

The problem in the previous treatment of raw spectral images is that the geometric transformation made to make them register with the preexposed flat fields is not sufficiently exact. The reseau marks (hardware dots on the detector), originally intended as reference points, were found too difficult to use together with complex spectra. Instead, indirect information, such as camera temperature measurements, is used to compute the geometric transform (Thompson, Turnrose, & Bohlin 1982). However, since the flat fields show strong pixel-to-pixel sensitivity variations of typically 10%, a mismatch of only one pixel may result in significant photometric errors.

A1.3. *Flat-Field Studies*

An initial study of the flat fields originally used was made by Dravins & Linde (1980). Subsequently, the latest available data from the LWR camera, recorded to generate the revised photometric calibration (intensity transfer function; ITF2) were used. They were geometrically transformed using the reseau marks as reference. An inspection shows various irregularities: in addition to general sensitivity variations, a moiré-like pattern is present, in the form of streaks of locally lowered pixel-to-pixel contrast. By numerically simulating the geometrical transform process, we reproduced the same moiré-type patterns in the output image. These smoothed streaks are due to the bilinear pixel interpolation and resampling in the geometric translation: IUESIPS performs a *double* resampling of the flat fields, once when they are created, and the second time when they are applied to calibrate the exposures. This results in considerable spatial smoothing, explaining why the fixed pattern noise is not well removed. (The software has changed during the years, and some of these problems are more pronounced in the IUESIPS version in use since 1981.) For a description of how the intensity transfer functions are generated, and for samples of the pixel-to-pixel variations, see, e.g., Bohlin et al. (1980).

A2. OUTLINE OF THE LUND METHOD

By comparing raw and flat-field images, it was noted that the fixed pattern in the interorder background of the raw images was identifiable also in the flat field, being a reflection of varying pixel-to-pixel sensitivity and/or zero-exposure level. Thus, from spatial correlations between the raw and flat-field images, the necessary geometric transformation could be measured. Then it also became possible to use a denser grid of correlation areas, and the reseau marks never needed to be used. The optimum identification of fixed patterns in *IUE* images is discussed in more detail by De La Peña (1989).

The following are the major steps of the Lund method:

(*a*) Selection of small subimages in the interorder background of each raw spectral image.

(*b*) Pattern matching between these subimages and a flat field corresponding to the raw image's actual exposure level, giving the relative geometric displacement vector for each subimage.

(*c*) Smoothing the displacement vector data to obtain a "rubber sheet" for the nonlinear geometric image stretching.

(*d*) Simultaneous geometric transformation and photometric calibration of the raw image. For the mapping to intensity space, the sensitivity curve for each pixel (ITF) is represented by a cubic spline fitted to the 12 flat-field levels.

(*e*) Identifying and removing those pixels which are affected by cosmic-ray events, transient detector readout noise (microphonics), or other data disturbances.

(*f*) Extraction of the spectrum and its adjacent background from a suitably rotated and magnified image. A matched slit tracks the exposed spectrum within a fraction of a pixel, and the weighting function perpendicular to the spectrum corresponds to the instrumental profile in that direction.

After the initial presentation of this technique (Linde & Dravins 1988), it became clear that further important gains in signal-to-noise ratio could be achieved by reconstructing the *IUE* flat-field calibration images in an optimal way. Thus, the commonly used set of pixel sensitivity maps of ITF2 is *not* utilized here (since these are already affected by one step of geometric resampling), but rather the original flat-field floodlamp *raw exposures*, from which the ITF2 data set had been synthesized. Actually, for the parts of the LWR detector used here, a very high degree of geometric stability was found in the component flat-field images, allowing a new set of ITF pixel sensitivity maps (images) to be generated without any geometrical resampling at all. A similar, but more generalized, procedure has been applied by Shaw (1990).

Relative to the new, unsmoothed, ITF images, the remaining necessary geometric correction needed before applying them to our LWR exposures was generally very small. In fact, throughout the period 1979–1989 most of our Mg II line observations in spectral order No. 83 needed shifts of less than 0.2 pixels. The same line in order No. 82 showed in a few cases a larger shift ($\lesssim$1.0 pixels).

A2.1. *Detection of Faint Spectral Features*

A comparison between this Lund method and IUESIPS has been made (Linde & Dravins 1990) by using each to analyze the same β Hyi exposures, and an example of the image processing phase is shown in Figure 6. This is a fraction of one high-dispersion image of β Hyi (LWR 17575) around the Mg II *k* emission in spectral order No. 83. The raw image (*top*) is seen following its geometric and photometric processing with the standard IUESIPS software (*center*), and after processing with the Lund method (*bottom*). The same contrast is used for all three images. The improved noise level resulting from the Lund method is especially valuable for studies of faint features at low exposure levels, e.g., feeble chromospheric emissions.

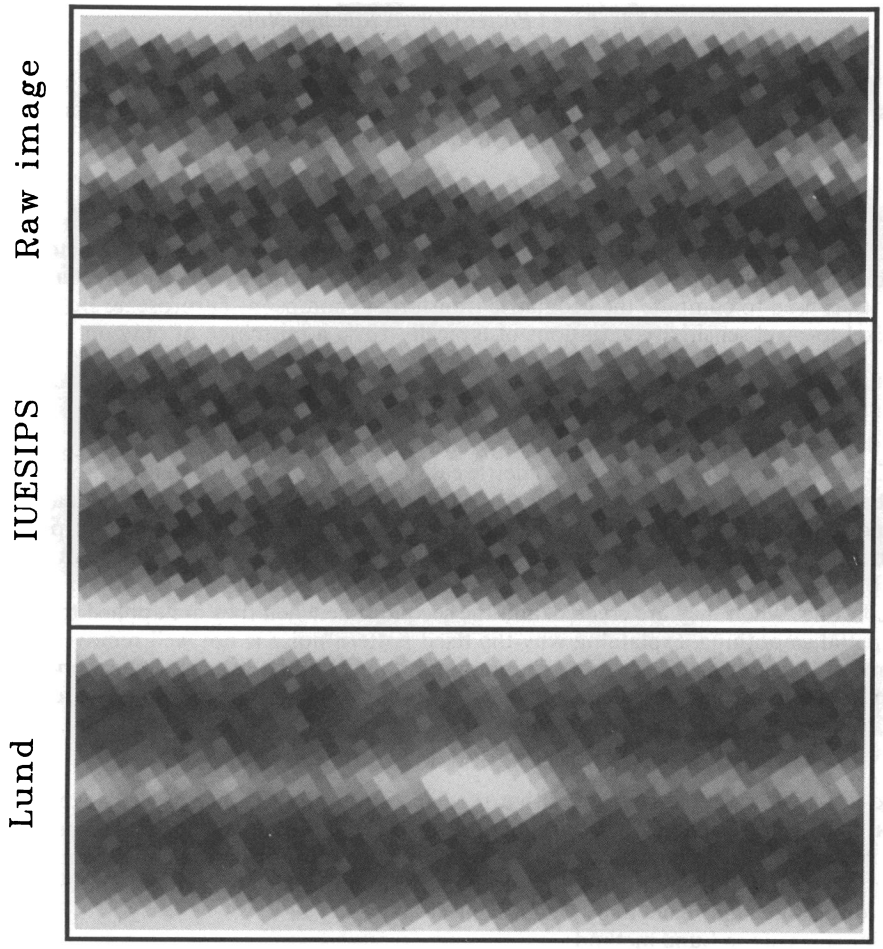

FIG. 6.—Careful processing of *IUE* images permits more accurate spectrophotometry than standard methods. A part of a spectral image of β Hyi is shown around its Mg II *k* emission. The raw image (*top*) is seen following its processing with the standard *IUE* software (center), and with the Lund method (*bottom*). The latter reduces the noise thanks to an accurate matching of the data with the small-scale sensitivity patterns on the detector.

A2.2. *Averaging Exposures*

If the remaining noise is random, averaging many spectra should improve the signal-to-noise ratio with a factor $\sqrt{N}$. Due to remnant systematic errors, this is not commonly the case for IUESIPS processed spectra, as has been verified by several authors (York & Jura 1982; Ayres 1990). A sequence of plots of the average of successively larger numbers of spectra (up to 45) is shown in Linde & Dravins (1990), both as obtained with IUESIPS, and with the Lund method. The noise in the Lund-processed spectra indeed seems to decrease approximately as $1/\sqrt{N}$, while remaining fixed-pattern noise causes a slower decrease in the IUESIPS case. Such analyses demonstrate how the detection of feeble stellar variability requires *both* the averaging of several exposures, *and* an optimum processing of the data.

A3. FURTHER DEVELOPMENTS

This technique has been further refined by the *IUE* image processing group at Goddard Space Flight Center, most importantly by generalizing it to all *IUE* observing modes (De La Peña et al. 1990; Nichols-Bohlin, De La Peña, & Shaw 1990). As a consequence, it has recently been adopted by NASA and ESA in the new software for the reprocessing of the entire *IUE* data archive.

REFERENCES

Allocchio, C., Morossi, C., & Vladilo, G. 1984, A&A, 130, 410
Altamore. A., Rossi, C., Rossi, L., & Villada de Arnedo, M. 1990, A&A, 234, 332
Avrett, E. H., Fontenla, J. M., & Loeser, R. 1992, in IAU Symp. 154, Infrared Solar Phys., ed. D. M. Rabin & J. T. Jefferies (Dordrecht: Kluwer), in press
Ayres, T. R. 1990, PASP, 102, 1420
Ayres, T. R., Fleming, T. A., & Schmitt, J. H. M. M. 1991, ApJ, 376, L45
Baliunas, S. L., & Vaughan, A. H. 1985, ARA&A, 23, 379
Barry, D. C., Cromwell, R. H., & Hege, E. K. 1987, ApJ, 315, 264
Beckers, J. M., Bridges, C. A., & Gilliam, L. B. 1976, A High Resolution Spectral Atlas of the Solar Irradiance from 380 to 700 Nanometers, (Sunspot, NM: Sacramento Peak Observatory)
Beckman, J., Crivellari, L., & Foing, B. 1984, ESO Messenger, 38, 24
Bohlin, R. C., Holm, A. V., Savage, B. D., Snijders, M. A. J., & Sparks, W. M. 1980, A&A, 85, 1
Bonnet, R. M. 1981, Space Sci. Rev., 29, 131

Bzowski, M. 1988, Acta Astron., 38, 443
Cayrel, R., Cayrel de Strobel, G., Campbell, B., Mein, N., Mein, P., & Dumont, S. 1983, A&A, 123, 89
Cram, L. E., & Mullan, D. J. 1985, ApJ, 294, 626
Crivellari, L., Franco, M. L., Molaro, P., Vladilo, G., & Beckman, J. E. 1983, A&AS, 52, 135
Danks, A. C., & Lambert, D. L. 1985, A&A, 148, 293
De La Peña, M. D. 1989, *IUE* NASA Newsletter, 38, 41
De La Peña, M. D., Shaw, R. A., Linde, P., & Dravins, D. 1990, in Evolution in Astrophysics, IUE Astronomy in the Era of New Space Missions (ESA SP-310), 617
Dobson, A. K., Donahue, R. A., Radick, R. R., & Kadlec, K. L. 1990, in Cool Stars, Stellar Systems, and the Sun, ed. G. Wallerstein (ASPC 9), 132
Dravins, D. 1990, in Evolution in Astrophysics, *IUE* Astronomy in the Era of New Space Missions (ESA SP-310), 61
Dravins, D., & Linde, P. 1980, in *IUE* Data Reduction, ed. W. W. Weiss et al., Vienna, 85
Dravins, D., Linde, P., Ayres, T. R., Linsky, J. L., Monsignori-Fossi, B., Simon, T., & Wallinder, F. 1993b, ApJ, 403, 412 (Paper III)
Dravins, D., Lindegren, L., Nordlund, Å., & VandenBerg, D. A. 1993a, ApJ, 403, 385 (Paper I)
Duncan, D. K., et al. 1991, ApJS, 76, 383
Foing, B. H., Crivellari, L., Vladilo, G., Rebolo, R., & Beckman, J. E. 1989, A&AS, 80, 189
Franco, M. L., Crivellari, L., Molaro, P., Vladilo, G., Ramella, M., Morossi, C., Allocchio, C., & Beckman, J. E. 1984, A&AS, 58, 693
García-Alegre, M. C., Ponz, J. D., & Vázquez, M. 1981, A&A, 96, 17
Génova, R., Beckman, J. E., Vladilo, G., & Molaro, P. 1989, Ap&SS, 156, 243
Génova, R., Molaro, P., Vladilo, G., & Beckman, J. E. 1990, ApJ, 355, 150
Gilliland, R. L., & Baliunas, S. L. 1987, ApJ, 314, 766
Gurzadyan, G. A. 1984, Zvezdnye Hromosfery ili Dublet 2800 Å Mg II v Astrofizike (Stellar Chromospheres or the 2800 Å Mg II Doublet in Astrophysics; in Russian) (Moscow: Nauka)
Hall, L. A. 1983, J. Geophys. Res., 88, 6797
Harris, A. W., & Sonneborn, G. 1987, in Exploring the Universe with the *IUE* Satellite, ed. Y. Kondo (Dordrecht: Reidel), 345
Harvey, J. W. 1984, in Solar Irradiance Variations on Active Region Time Scales, ed. B. J. LaBonte, G. A. Chapman, H. S. Hudson, & R. C. Willson (NASA CP-2310), 197
Heath, D. F., & Schlesinger, B. M. 1986, J. Geophys. Res., 91, 8672
Keil, S. L., & Worden, S. P. 1984, ApJ, 276, 766
Kinney, A. L., Bohlin, R. C., & Neill, J. D. 1991, PASP, 103, 694
Kohl, J. L., & Parkinson, W. H. 1976, ApJ, 205, 599
Kohl, J. L., Parkinson, W. H., & Kurucz, R. L. 1978, Center and Limb Solar Spectrum in High Spectral Resolution 225.2 nm to 319.6 nm (Cambridge: Harvard-Smithsonian Center for Astrophysics)
Kurucz, R. L., Furenlid, I., Brault, J., & Testerman, L. 1984, Solar Flux Atlas From 296 to 1300 nm (Sunspot, NM: National Solar Observatory)
Lean, J. L. 1984, J. Geophys. Res., 89, 1
———. 1987, J. Geophys. Res., 92, 839
———. 1990, J. Geophys. Res., 95, 11933
Lemaire, P., & Skumanich, A. 1973, A&A, 22, 61
Lind, J., & Dravins, D. 1980, A&A, 90, 151
Linde, P., & Dravins, D. 1988, in A Decade of UV Astronomy with *IUE* (ESA SP-281), Vol. 2, 345
Linde, P., & Dravins, D. 1990, in Evolution in Astrophysics, *IUE* Astronomy in the Era of New Space Missions (ESA SP-310), 605
Linsky, J. L., Hunten, D. M., Sowell, R., Glackin, D. L., & Kelch, W. L. 1979a, ApJS, 41, 481
Linsky, J. L., Worden, S. P., McClintock, W., & Robertson, R. M. 1979b, ApJS, 41, 47
Molaro, P., Vladilo, G., & Beckman, J. E. 1986, A&A, 161, 339
Mullan, D. J. 1984, ApJ, 284, 769
Nichols-Bohlin, J., De La Peña, M. D., & Shaw, R. A. 1990, in Evolution in Astrophysics, *IUE* Astronomy in the Era of New Space Missions (ESA SP-310), 623
Oranje, B. J. 1983a, A&A, 122, 88
———. 1983b, A&A, 124, 43
Pasquini, L., & Pallavicini, R. 1991, A&A, 251, 199
Pasquini, L., Pallavicini, R., & Pakull, M. 1988, A&A, 191, 253
Rebolo, R., García Lopez, R., Beckman, J. E., Vladilo, G., Foing, B. H., & Crivellari, L. 1989, A&AS, 80, 135
Shcherbakov, A. G., & Shcherbakova, Z. A. 1991, in IAU Colloq. 130, The Sun and Cool Stars: Activity, Magnetism, Dynamos, ed. I. Tuominen, D. Moss, & G. Rüdiger (Berlin: Springer), 252
Schrijver, C. J. 1987, A&A, 172, 111
———. 1988, A&A, 189, 163
Shaw, R. A. 1990, in Evolution in Astrophysics, *IUE* Astronomy in the Era of New Space Missions (ESA SP-310), 621
Sheeley, N. R. 1967, ApJ, 147, 1106
Simon, T., Herbig, G., & Boesgaard, A. M. 1985, ApJ, 293, 551
Sivaraman, K. R., Singh, J., Bagare, S. P., & Gupta, S. S. 1987, ApJ, 313, 456
Skumanich, A. 1972, ApJ, 171, 565
Skumanich, A., Lean, J. L., White, O. R., & Livingston, W. C. 1984, ApJ, 282, 776
Skumanich, A., & Lites, B. W. 1986, ApJ, 310, 419
Smith, M. A. 1983, AJ, 88, 1031
Soderblom, D. R. 1983, ApJS, 53, 1
Soderblom, D. R., Duncan, D. K., & Johnson, D. R. H. 1991, ApJ, 375, 722
Stencel, R. E., Mullan, D. J., Linsky, J. L., Basri, G. S., & Worden, S. P. 1980, ApJS, 44, 383
Stępień, K. 1989, Acta Astron., 39, 209
Thompson, R. W., Turnrose, B. E., & Bohlin, R. C. 1982, A&A, 107, 11
Vladilo, G., Beckman, J. E., Crivellari, L., Franco, M. L., & Molaro, P. 1985, A&A, 144, 81
Vladilo, G., Molaro, P., Crivellari, L., Foing, B. H., Beckman, J. E., & Genova, R. 1987, A&A, 185, 233
Warner, B. 1969, MNRAS, 144, 333
Weiler, E. J., & Oegerle, W. R. 1979, ApJS, 39, 537
White, O. R., & Livingston, W. C. 1981, ApJ, 249, 798
White, O. R., Livingston, W. C., & Wallace, L. 1987, J. Geophys. Res., 92, 823
Wilson, O. C. 1978, ApJ, 226, 379
Wolff, S. C., & Heasley, J. N. 1984, PASP, 96, 231
York, D. G., & Jura, M. 1982, ApJ, 254, 88
Zarro, D. M. 1983, ApJ, 267, L61
Zarro, D. M., & Rodgers, A. W. 1983, ApJS, 53, 815
Zirin, H. 1975, ApJ, 199, L63